Finite-Element Solution of Periodic Waveguides for Acoustic Waves

MASANORI KOSHIBA, SENIOR MEMBER, IEEE, SEIICHI MITOBE, AND MICHIO SUZUKI, SENIOR MEMBER, IEEE

Abstract—**A numerical approach based on the finite-element method is described for the analysis of periodic waveguides for acoustic waves. The validity of the method is confirmed by comparing the numerical results for the dispersion curves of horizontal shear (SH) waves in a groove grating on an isotropic material with the experimental results. The application of this approach is also demonstrated by investigating the propagation characteristics of SH surface waves in a groove grating on a layered isotropic material. Furthermore, for a groove grating on a piezoelectric material, the stop-band width and the center-frequency shift in the dispersion diagram for Rayleigh waves are calculated, which are important parameters for design of a reflector, and the influences of groove shape on these parameters are examined.**

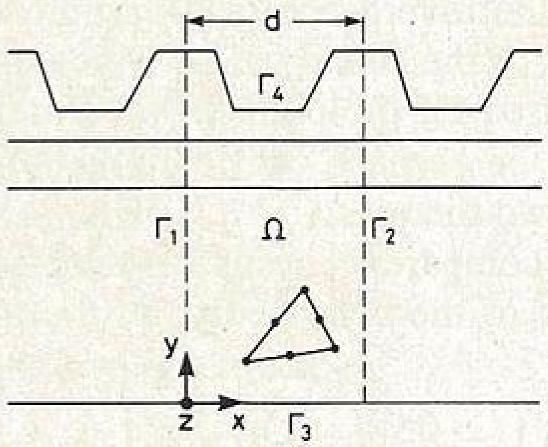

Fig. 1. Periodic waveguide.

I. Introduction

In recent years, attention has been given to the use of gratings on solid surfaces to reduce the propagation velocity of acoustic waves and to introduce bandgaps and cutoff frequencies into their dispersion relations for the purpose of producing delay lines and filtering devices [1]–[6]. Several methods for the analysis of periodic waveguides in Fig. 1 have been proposed, and the coupled-mode theory, which derives the coupled-mode equations under the assumption of small perturbations, is widely used [7]–[12]. The calculation procedure of this method is relatively simple, but the accuracy is degraded for large perturbations. On the other hand, it is possible to increase the accuracy by expanding the acoustic and electromagnetic fields in terms of Fourier series by means of the Floquet theorem and deriving the homogeneous linear equations of infinite order [13]–[19]. However, it seems to be difficult to apply this approach to arbitrarily shaped periodic waveguides.

In this paper a numerical approach based on the finite-element method is described for the analysis of arbitrarily shaped periodic waveguides for acoustic waves. The validity of the method is confirmed by comparing the numerical results for the dispersion curves of horizontal shear (SH) waves in a groove grating on an isotropic material with the experimental results [4]. We also demonstrate the application of this approach by investigating the propagation characteristics of SH surface waves in a groove grating on a layered isotropic material. Furthermore, for a groove grating on a piezoelectric material, the stop-band width and the center-frequency shift in the dispersion diagram for Rayleigh waves are calculated, which are important parameters for design of a reflector, and the influences of groove shape on these parameters are examined.

Manuscript received April 22, 1986; revised September 12, 1986.

The authors are with the Department of Electronic Engineering, Hokkaido University, Sapporo, 060 Japan.

IEEE Log Number 8612862.

II. Basic Equations

The structure under study is periodic in the x direction with period d as shown in Fig. 1. The region Ω surrounded by boundaries Γ_1 to Γ_4 is the basic cell. The mechanical boundary conditions on Γ_3 and Γ_4 are $u_x = u_y = u_z = 0$ or $T_{xn} = T_{yn} = T_{zn} = 0$, where u_x, u_y, and u_z are the particle displacements, T_{xn}, T_{yn}, and T_{zn} are the stresses, and n denotes the outward normal direction to the boundary. The electrical boundary conditions on Γ_3 and Γ_4 are $\phi = 0$ or $D_n = 0$, where ϕ is the electric potential and D_n is the electric displacement.

Assuming that no variation exists in the z direction, we have the following equations [1]:

$$\partial \boldsymbol{T}_x/\partial x + \partial \boldsymbol{T}_y/\partial y + \omega^2 \rho \boldsymbol{u} = 0 \tag{1a}$$

$$\partial D_x/\partial x + \partial D_y/\partial y = 0 \tag{1b}$$

where

$$\boldsymbol{u} = [u_x \quad u_y \quad u_z]^T \tag{2a}$$

$$\boldsymbol{T}_x = [T_{xx} \quad T_{yx} \quad T_{zx}]^T \tag{2b}$$

$$\boldsymbol{T}_y = [T_{xy} \quad T_{yy} \quad T_{zy}]^T. \tag{2c}$$

Here ω is the angular frequency, ρ is the mass density, and T denotes a transpose.

III. Finite-Element Approach

Dividing the region Ω into a number of second-order triangular elements in Fig. 1, $\boldsymbol{u}$ and ϕ within each element are defined in terms of the particle displacement and the electric potential at the corner and midside nodal points:

$$\boldsymbol{u} = [N]^T \{u\}_e \tag{3a}$$

$$\phi = \{N\}^T \{\phi\}_e \tag{3b}$$

where

$$[N] = \begin{bmatrix} \{N\} & \{0\} & \{0\} \\ \{0\} & \{N\} & \{0\} \\ \{0\} & \{0\} & \{N\} \end{bmatrix}. \tag{4}$$

Here $\{u\}_e$ and $\{\phi\}_e$ are the particle displacement and electric potential vectors corresponding to the nodal points within each element, respectively, $\{N\}$ is the shape function vector [20], [21], $\{0\}$ is a null vector, and $\{\cdot\}$ and $\{\cdot\}^T$ denote a column vector and a row vector, respectively.

The well-known constitutive relations for piezoelectric materials are written as [1], [20]

$$\boldsymbol{T} = [c]\boldsymbol{S} - [e]^T\boldsymbol{E} \tag{5a}$$

$$\boldsymbol{D} = [\epsilon]\boldsymbol{E} + [e]\boldsymbol{S} \tag{5b}$$

where $\boldsymbol{T}$, $\boldsymbol{S}$, $\boldsymbol{D}$, and $\boldsymbol{E}$ are the stress, strain, electric displacement, and electric field vectors, respectively, and $[c]$, $[e]$, and $[\epsilon]$ are the elastic constant, piezoelectric, and permittivity tensors, respectively.

The strain vector $\boldsymbol{S}$ and the electric field vector $\boldsymbol{E}$ are expressed as [20]

$$\boldsymbol{S} = [B_u]\{u\}_e \tag{6a}$$

$$\boldsymbol{E} = -[B_\phi]\{\phi\}_e \tag{6b}$$

where $[B_u]$ and $[B_\phi]$ are given by

$$[B_u] = \begin{bmatrix} \{N_x\} & \{0\} & \{0\} & \{0\} & \{0\} & \{N_y\} \\ \{0\} & \{N_y\} & \{0\} & \{0\} & \{0\} & \{N_x\} \\ \{0\} & \{0\} & \{0\} & \{N_y\} & \{N_x\} & \{0\} \end{bmatrix} \tag{7a}$$

$$[B_\phi] = [\{N_x\} \quad \{N_y\} \quad \{0\}]. \tag{7b}$$

Here $\{N_x\} \equiv \partial\{N\}/\partial x$ and $\{N_y\} \equiv \partial\{N\}/\partial y$.

Equation (5) is now expressed in terms of $\{u\}_e$ and $\{\phi\}_e$ as

$$\boldsymbol{T} = [c][B_u]\{u\}_e + [e]^T[B_\phi]\{\phi\}_e \tag{8a}$$

$$\boldsymbol{D} = -[\epsilon][B_\phi]\{\phi\}_e + [e][B_u]\{u\}_e. \tag{8b}$$

Using a Galerkin procedure on (1), we obtain

$$\iint_e [N](\partial\boldsymbol{T}_x/\partial x + \partial\boldsymbol{T}_y/\partial y + \omega^2\rho_e\boldsymbol{u})\, d\Omega = \{0\} \tag{9a}$$

$$\iint_e \{N\}(\partial D_x/\partial x + \partial D_y/\partial y)\, d\Omega = \{0\} \tag{9b}$$

where the integration is carried over the element subdomain Ω_e.

Integrating by parts, (9) becomes

$$\iint_e ([N_x]\boldsymbol{T}_x + [N_y]\boldsymbol{T}_y - \omega^2\rho_e[N]\boldsymbol{u})\, d\Omega - \int_e [N]\boldsymbol{T}_n\, d\Gamma = \{0\} \tag{10a}$$

$$\iint_e (\{N_x\}D_x + \{N_y\}D_y)\, d\Omega - \int_e \{N\}D_n\, d\Gamma = \{0\} \tag{10b}$$

where $[N_x] \equiv \partial[N]/\partial x$, $[N_y] \equiv \partial[N]/\partial y$, $\boldsymbol{T}_n = [T_{xn} \quad T_{yn} \quad T_{zn}]^T$, and the second integration on the left-hand side is carried over the contour Γ_e of the region Ω_e.

Noting that $\boldsymbol{T}_n$ and D_n are continuous across Γ_e (boundary conditions at the interface between two different media) and considering the boundary conditions on Γ_3 and Γ_4 (See Section II), from (3), (8), and (10) the following global matrix equation is derived:

$$\begin{bmatrix} [K] & [C] \\ [C]^T & -[G] \end{bmatrix}\begin{bmatrix} \{u\} \\ \{\phi\} \end{bmatrix} - \omega^2\begin{bmatrix} [M] & [0] \\ [0] & [0] \end{bmatrix}\begin{bmatrix} \{u\} \\ \{\phi\} \end{bmatrix} = \begin{bmatrix} \sum_{i=1}^{2}(-1)^i \sum_e' \int_e [N]\boldsymbol{T}_x|_{\Gamma_i}\, dy \\ \sum_{i=1}^{2}(-1)^i \sum_e' \int_e \{N\}D_x|_{\Gamma_i}\, dy \end{bmatrix} \tag{11}$$

where

$$[K] = \sum_e \iint_e [B_u][c]_e[B_u]^T\, dx\, dy \tag{12a}$$

$$[C] = \sum_e \iint_e [B_u][e]_e^T[B_\phi]^T\, dx\, dy \tag{12b}$$

$$[G] = \sum_e \iint_e [B_\phi][\epsilon]_e[B_\phi]^T\, dx\, dy \tag{12c}$$

$$[M] = \sum_e \iint_e \rho_e[N][N]^T\, dx\, dy. \tag{12d}$$

Here $\{u\}$ is the nodal particle displacement vector, $\{\phi\}$ is the nodal electric potential vector, $[0]$ is a null matrix, and Σ_e and Σ_e' extend over all different elements and the elements related to the boundaries Γ_1 and Γ_2, respectively. Constraints on the stress and the electric displacement on Γ_3 and Γ_4 are natural boundary conditions and will be automatically satisfied. Constraints on the particle displacement and the electric potential on Γ_3 and Γ_4 may be imposed simply by deleting a row and a column of the relevant element matrices.

The periodic conditions are given by

$$u|_{\Gamma_2} = pu|_{\Gamma_1} \tag{13a}$$

$$T_x|_{\Gamma_2} = pT_x|_{\Gamma_1} \tag{13b}$$

$$\phi|_{\Gamma_2} = p\phi|_{\Gamma_1} \tag{13c}$$

$$D_x|_{\Gamma_2} = pD_x|_{\Gamma_1} \tag{13d}$$

where

$$p = \exp(-j\beta d). \tag{14}$$

Here β is the phase constant in the x direction.

Using (13), from (11) we obtain

$$\begin{bmatrix} [\tilde{K}] & [\tilde{C}] \\ [\tilde{C}]^\dagger & -[\tilde{G}] \end{bmatrix} \begin{bmatrix} \{\tilde{u}\} \\ \{\tilde{\phi}\} \end{bmatrix} - \omega^2 \begin{bmatrix} [\tilde{M}] & [0] \\ [0] & [0] \end{bmatrix} \begin{bmatrix} \{\tilde{u}\} \\ \{\tilde{\phi}\} \end{bmatrix} = \{0\} \tag{15}$$

where

$$\{\tilde{u}\} = \begin{bmatrix} \{u\}_0 \\ \{u\}_1 \end{bmatrix} \tag{16}$$

$$\{\tilde{\phi}\} = \begin{bmatrix} \{\phi\}_0 \\ \{\phi\}_1 \end{bmatrix} \tag{17}$$

$$[\tilde{K}] = \begin{bmatrix} [K]_{00} & [K]_{01} + p[K]_{02} \\ [K]_{10} + p^*[K]_{20} & [K]_{11} + [K]_{22} + p[K]_{12} + p^*[K]_{21} \end{bmatrix}. \tag{18}$$

Here the components of the $\{u\}_1$ and $\{\phi\}_1$ vectors are the values of the particle displacement and the electric potential at nodal points on the boundary Γ_1, respectively; the components of the $\{u\}_0$ and $\{\phi\}_0$ vectors are the values of the particle displacement and the electric potential at nodal points in the interior region except the boundaries Γ_1 and Γ_2, respectively; the matrices $[\tilde{C}]$, $[\tilde{G}]$, and $[\tilde{M}]$, are given by replacing K in (18) by C, G, and M, respectively; * and † denote a complex conjugate and a complex conjugate transpose, respectively; and $[K]_{00}$, $[K]_{01}$, $\cdots$, and $[K]_{22}$ are the submatrices of $[K]$:

$$[K] = \begin{bmatrix} [K]_{00} & [K]_{01} & [K]_{02} \\ [K]_{10} & [K]_{11} & [K]_{12} \\ [K]_{20} & [K]_{21} & [K]_{22} \end{bmatrix}. \tag{19}$$

Eliminating $\{\phi\}$ from (15), we obtain the following final eigenvalue equation:

$$([\tilde{K}] + [\tilde{C}][\tilde{G}]^{-1}[\tilde{C}]^\dagger)\{u\} - \omega^2[\tilde{M}]\{u\} = \{0\}. \tag{20}$$

This equation determines the propagation characteristics of periodic waveguides. In the present analysis, the Cholesky method, the Householder's method, the method of bisections, and the method of inverse iterations are suitably used for solving (20).

IV. Computed Results

First, we consider a groove grating on an isotropic material. Fig. 2 shows the dispersion curves of SH waves of an isotropic waveguide with rectangular grooves, where $k_s = \omega/v_s$ and v_s is the bulk shear wave velocity. Our results agree well with the experimental results [4]. Comparison of the results in Fig. 2(a) and (b) shows that the deeper grooves give a greatly increased amount of wave slowing.

Fig. 3 shows the dispersion curve of the fundamental SH surface wave of a layered isotropic waveguide with rectangular grooves, where $k_{s1} = \omega/v_{s1}$, and v_{s1} and v_{s2} are the bulk shear wave velocities of the substrate and the film, respectively. The phase velocity of this SH surface wave is lower than that of the fundamental Love wave and, for large βd, this velocity may become even lower than the bulk shear wave velocity of the film (v_{s2}).

Next we consider a groove grating on a piezoelectric material (Y–Z $LiNbO_3$) and investigate the stop-band width and the center-frequency shift at $\beta d = \pi$ (the first Bragg reflection) in the dispersion diagram for Rayleigh waves. In the case of Rayleigh waves, we set $u_x = u_y = u_z = D_y = 0$ on the boundary Γ_3 in Fig. 1 [20].

Fig. 4 shows the normalized stop-band width $\Delta F/f_0$ and the normalized center-frequency shift $\Delta f/f_0$ of a piezoelectric waveguide with rectangular grooves, where $\Delta F/f_0$, $\Delta f/f_0$, and f_0 are given by

$$\Delta F/f_0 = (f_u - f_l)/f_0 \tag{21}$$

$$\Delta f/f_0 = [(f_u + f_l)/2 - f_0]/f_0 \tag{22}$$

$$f_0 = v_R/2d. \tag{23}$$

Here f_u and f_l are the upper and lower bound frequencies of the stop band, respectively, and v_R is the velocity of the Rayleigh wave on a Y–Z $LiNbO_3$ substrate. In Fig. 4 the groove width is one-half of the period d, the groove depth h is varied, and the substrate thickness is about five times the period d. Our results for the center-frequency shift agree well with the experimental results [6].

Lastly, we examine the influences of groove shape on the stop-band width and the center-frequency shift of the groove grating on Y–Z $LiNbO_3$. Fig. 5 shows $\Delta F/f_0$ and

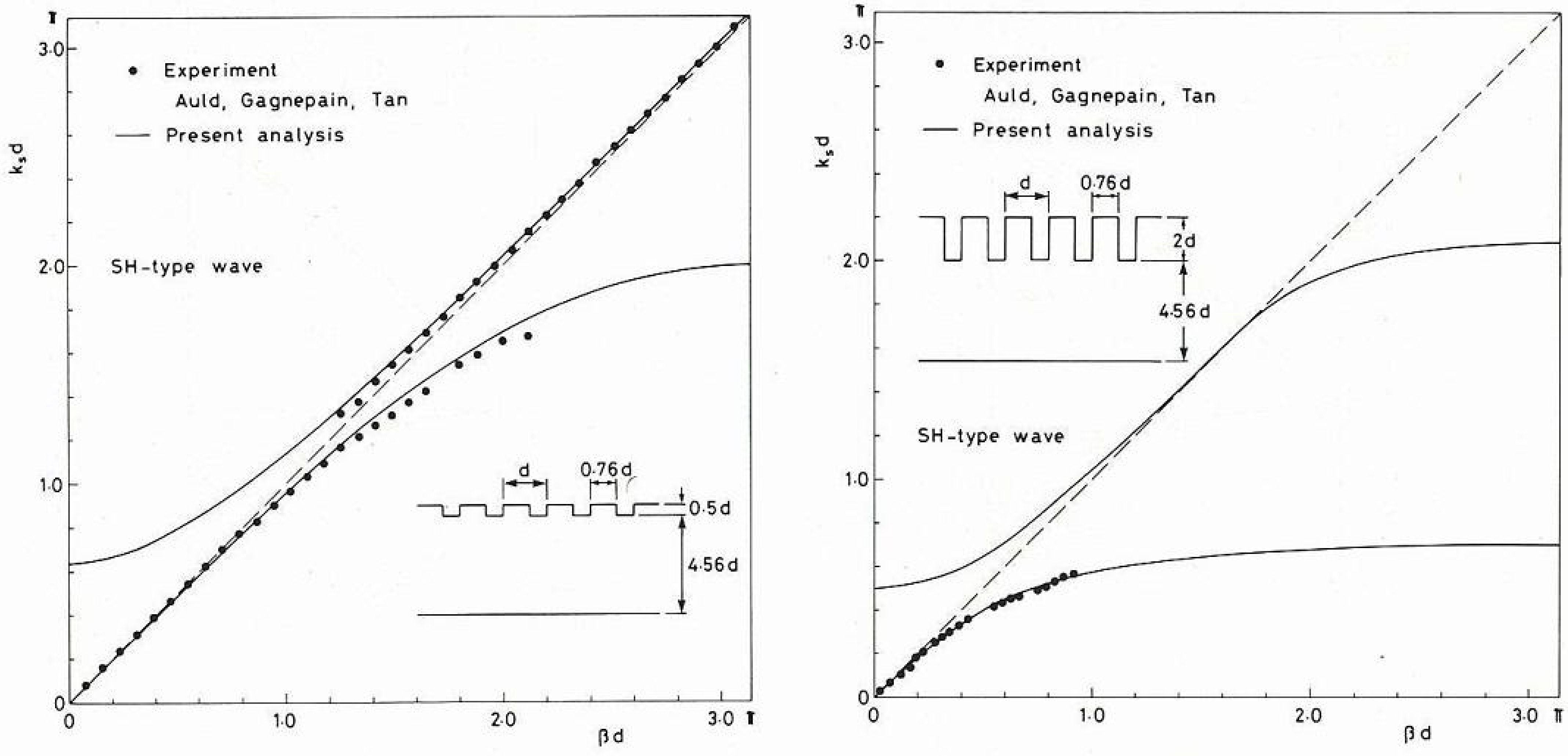

(a) (b)

Fig. 2. Dispersion curves of SH waves of isotropic waveguide with rectangular grooves. (a) Shallow groove. (b) Deep groove.

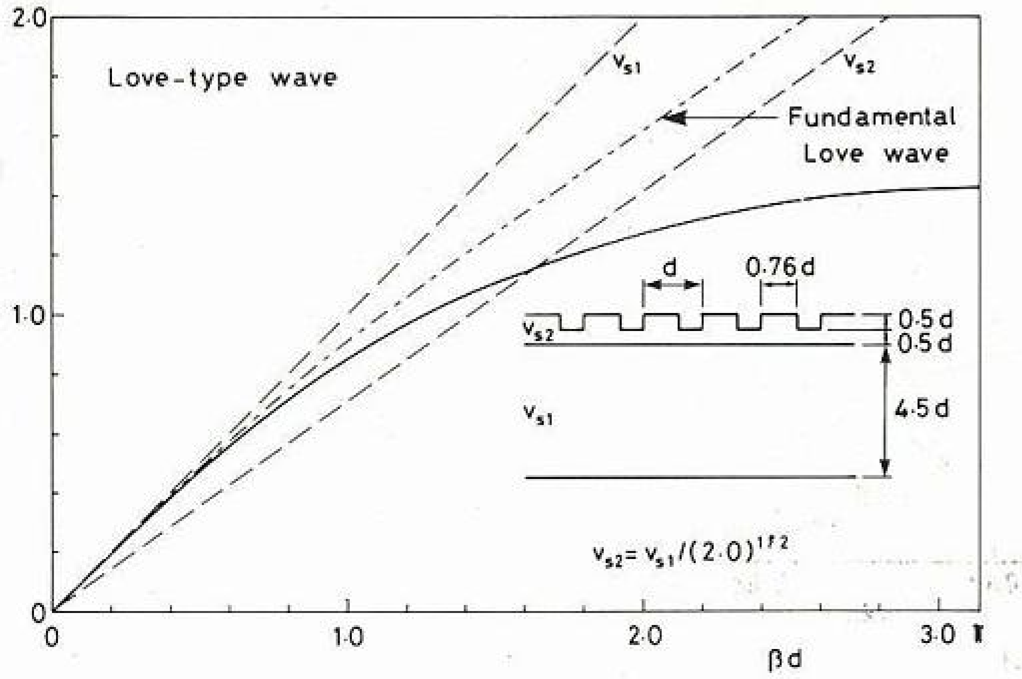

Fig. 3. Dispersion curve of fundamental SH surface wave of layered isotropic waveguide with rectangular grooves.

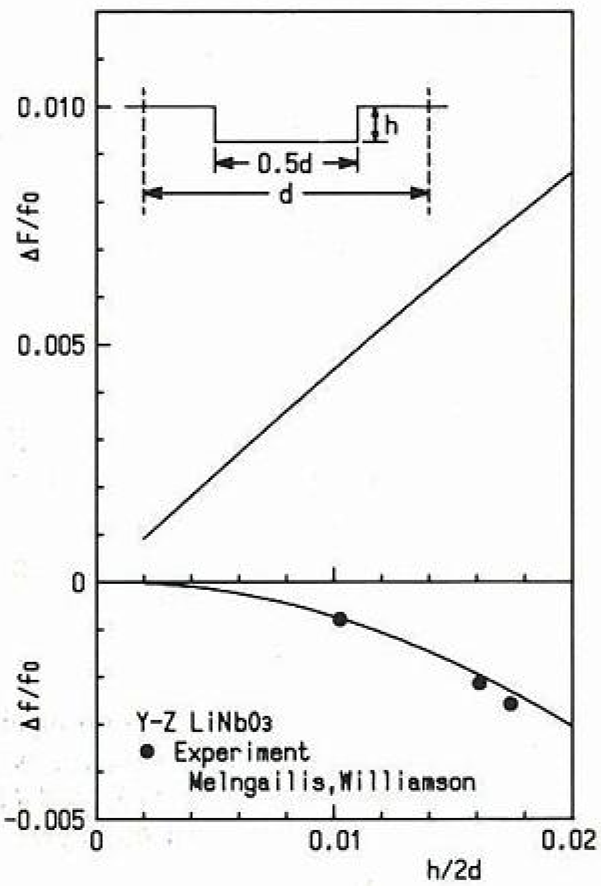

Fig. 4. Stop-band width and center-frequency shift for Rayleigh wave of piezoelectric waveguide with rectangular grooves.

$\Delta f/f_0$ at $\beta d = \pi$ of a piezoelectric waveguide with trapezoidal grooves ($\theta \neq 0$), where dashed lines are for the rectangular grooves ($\theta = 0$) and are the same as the solid lines in Fig. 4. It is found from Fig. 5 that the center-frequency shift is decreased as θ becomes larger. This is due to the fact that for large θ, namely, a gentle slope, the energy storage effect [3] becomes smaller. When the area of trapezoidal groove (S_t) is larger than that of rectangular groove (S_r), namely, $S_t > S_r$ in Fig. 5 (a), the stop-band width for trapezoidal grooves is smaller than that for rectangular grooves. Also, as θ becomes larger, the stop-band width is decreased. When $S_t = S_r$ in Fig. 5(b), the influence of θ on the stop-band width is extremely small. When $S_t < S_r$ in Fig. 5(c), the stop-band width for trapezoidal grooves is slightly larger than that for rectangular grooves. For very large θ (for example, $\theta = 80°$), however, the stop-band width for trapezoidal grooves becomes smaller than that for rectangular grooves.

V. Conclusion

A method of analysis based on the finite-element method was developed for the solution of the propagation problem in periodic waveguides for acoustic waves. Numerical examples are presented for the groove gratings for SH waves and Rayleigh waves. This approach can be easily applied to the metallic gratings [2], [5], [7], [8], [13]–[16], [19].

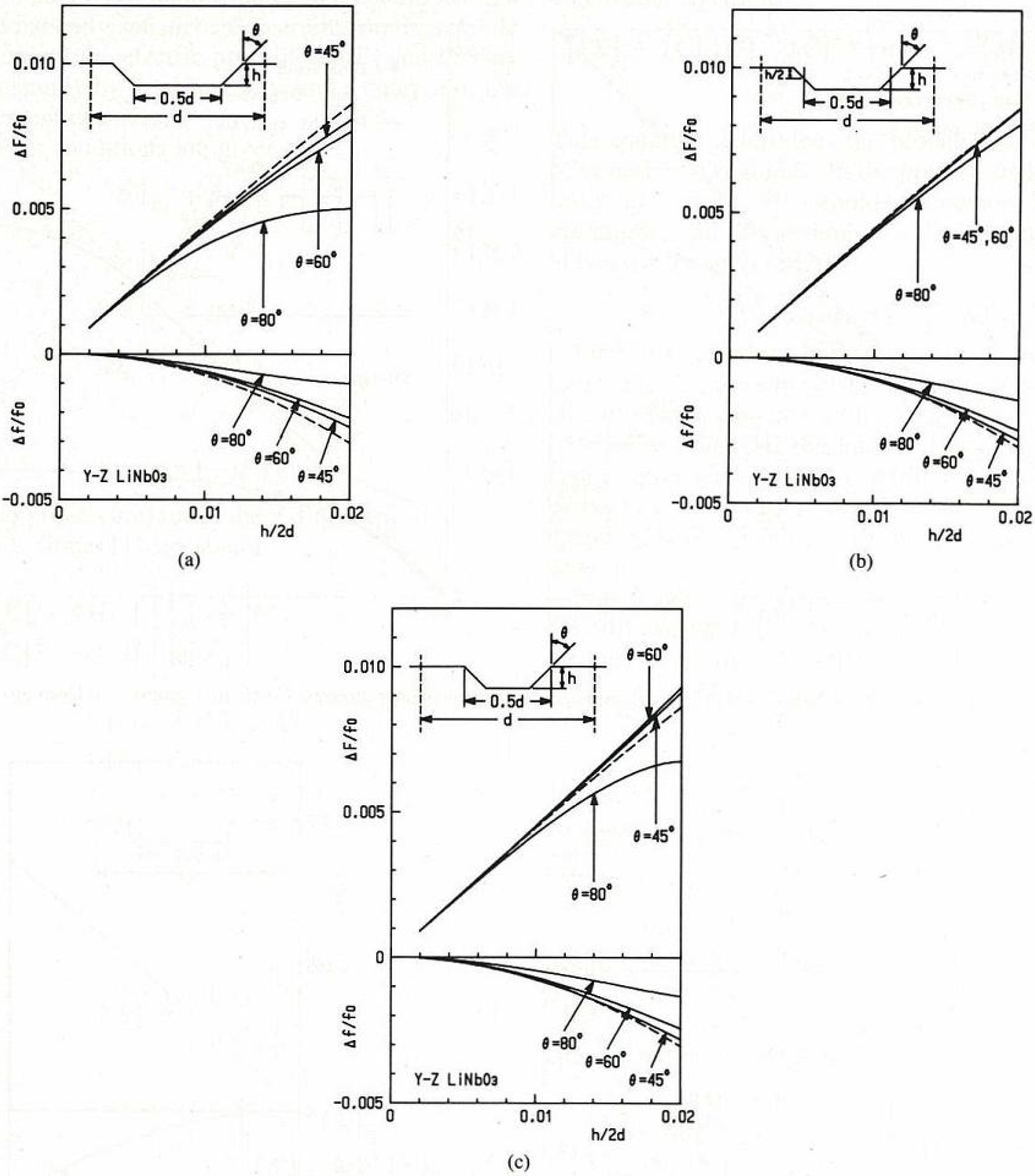

Fig. 5. Stop-band width and center-frequency shift for Rayleigh wave of piezoelectric waveguide with trapezoidal grooves. (a) $S_t > S_r$. (b) $S_t = S_r$. (c) $S_t < S_r$ (S_t and S_r are areas of trapezoidal and rectangular grooves, respectively).

REFERENCES

[1] B. A. Auld, *Acoustic Fields and Waves in Solids*, vols. I and II. New York: Wiley-Interscience, 1973.

[2] H. Matthews, Ed., *Surface Wave Filters*. New York: Wiley-Interscience, 1977.

[3] R. C. M. Li and J. Melngailis, "The influence of stored energy at step discontinuities on the behavior of surface-wave gratings," *IEEE Trans. Sonics Ultrason.*, vol. SU-22, pp. 189–198, May 1975.

[4] B. A. Auld, J. J. Gagnepain, and M. Tan, "Horizontal shear surface waves on corrugated surfaces," *Electron. Lett.*, vol. 12, pp. 650–652, Nov. 1976.

[5] S. Urabe, Y. Koyamada, and S. Yoshikawa, "Experiments on metallic-strip-grating for SAW reflector," *Trans. Inst. Electron. Commun. Eng. Japan*, vol. J60-A, pp. 875–876, Sept. 1977 (in Japanese).

[6] J. Melngailis and R. C. Williamson, "Interaction of surface waves and bulk waves in gratings: Phase shifts and sharp surface-wave/reflected bulk wave resonators," in *1978 Ultrason. Symp. Proc.*, 1978, pp. 623–629.

[7] Y. Suzuki and H. Shimizu, "Reflection of surface acoustic waves due to piezoelectric and elastic perturbation by periodic strip electrodes and its applications to resonators," *Inst. Electron. Commun. Eng. Japan*, Tech. Res. Rep.US74-45, Jan. 1975 (in Japanese).

[8] Y. Suzuki, H. Shimizu, M. Takeuchi, K. Nakamura, and A. Yamada, "Some studies on SAW resonators and multiple-mode filters," in *1976 Ultrason. Symp. Proc.*, 1976, pp. 33–38.

[9] S. R. Seshadri, "Love wave interaction in a thin film with a periodic surface corrugation," *IEEE Trans. Sonics Ultrason.*, vol. SU-25, pp. 378–383, Nov. 1978.

[10] ——, "Effect of periodic surface corrugation on the propagation of Rayleigh waves," *J. Acoust. Soc. Amer.*, vol. 65, pp. 687–694, Mar. 1979.

[11] M. Tsutsumi and N. Kumagai, "Behavior of Bleustein-Gulyaev waves in a periodically corrugated piezoelectric crystal," *IEEE Trans. Microwave Theory Tech.*, vol. MTT-28, pp. 627–632, June 1980.

[12] H. A. Haus and P. V. Wright, "The analysis of grating structures by coupling-of-modes theory," in *1980 Ultrason. Symp. Proc.*, 1980, pp. 277–281.

[13] S. G. Joshi and R. M. White, "Dispersion of surface elastic waves produced by a conducting grating on a piezoelectric crystal," *J. Appl. Phys.*, vol. 39, pp. 5819–5827, Dec. 1968.
[14] K. Bløtekjær, K. A. Ingebrigtsen, and H. Skeie, "A method for analyzing waves in structures consisting of metal strips on dispersive media," *IEEE Trans. Electron Devices*, vol. ED-20, pp. 1133–1138, Dec. 1973.
[15] —, "Acoustic surface waves in piezoelectric materials with periodic metal strips on the surface," *IEEE Trans. Electron Devices*, vol. ED-20, pp. 1139–1146, Dec. 1973.
[16] S. Datta and B. J. Hunsinger, "An analytical theory for the scattering of surface acoustic waves by a single electrode in a periodic array on a piezoelectric substrate," *J. Appl. Phys.*, vol. 51, pp. 4817–4823, Sept. 1980.
[17] N. E. Glass and A. A. Maradudin, "Shear surface elastic waves on large amplitude gratings," *Electron. Lett.*, vol. 17, pp. 773–774, Oct. 1981.
[18] J. Z. Wilcox, K. H. Yen, T. J. Wilcox, and G. Evans, "Horizontal shear acoustic waves on layered surfaces with sinusoidal corrugations," *J. Appl. Phys.*, vol. 53, pp. 2862–2870, Apr. 1982.
[19] E. J. Danicki, "Propagation of transverse surface acoustic waves in rotated *Y*-cut quartz substrates under heavy periodic metal electrodes," *IEEE Trans. Sonics Ultrason.*, vol. SU-30, pp. 304–312, Sept. 1983.
[20] Y. Kagawa and T. Yamabuchi, "A finite element approach to electromechanical problem with an application to energy-trapped and surface-wave devices," *IEEE Trans. Sonics Ultrason.*, vol. SU-23, pp. 263–272, July 1976.
[21] M. Koshiba, S. Karakida, and M. Suzuki, "Finite-element analysis of Lamb wave scattering in an elastic plate waveguide," *IEEE Trans. Sonics Ultrason.*, vol. SU-31, pp. 18–25, Jan. 1984.

Masanori Koshiba (SM'84), for a photograph and biography please see p. 466 of this TRANSACTIONS.

Seiichi Mitobe was born in Kamifurano, Japan, on January 7, 1960. He received the B.S. and M.S. degrees in electronic engineering from Hokkaido University, Sapporo, Japan, in 1983 and 1985, respectively. He is presently studying toward the Ph.D. degree in electronic engineering at Hokkaido University.

Mr. Mitobe is a member of the Institute of Electronics and Communication Engineers of Japan.

Michio Suzuki (SM'57), for a photograph and biography please see page 466 of this TRANSACTIONS.